Anomalous Manganese Activation of a Pyrophosphate Cathode in Sodium Ion Batteries: A Combined Experimental and Theoretical Study

Chan Sun Park,[†,∥] Heejin Kim,[†,∥] Rana A. Shakoor,[§,∥] Eunjeong Yang,[†] Soo Yeon Lim,[†] Ramazan Kahraman,[§] Yousung Jung,*[,†,‡] and Jang Wook Choi*[,†,‡]

[†]Graduate School of EEWS (WCU) and [‡]KAIST Institute NanoCentury, Korea Advanced Institute of Science and Technology (KAIST), Yuseong-gu, Daejeon 305-701, Republic of Korea

[§]Department of Chemical Engineering, College of Engineering, Qatar University 2713, Doha, Qatar

S Supporting Information

ABSTRACT: Sodium ion batteries (SIBs) have many advantages such as the low price and abundance of sodium raw materials that are suitable for large-scale energy storage applications. Herein, we report an Mn-based pyrophosphate, $Na_2MnP_2O_7$, as a new SIB cathode material. Unlike most Mn-based cathode materials, which suffer severely from sluggish kinetics, $Na_2MnP_2O_7$ exhibits good electrochemical activity at ~3.8 V vs Na/Na+ with a reversible capacity of 90 mAh g−1 at room temperature. It also shows an excellent cycling and rate

performance: 96% capacity retention after 30 cycles and 70% capacity retention at a c-rate increase from 0.05C to 1C. These electrochemical activities of the Mn-containing cathode material even at room temperature with relatively large particle sizes are remarkable considering an almost complete inactivity of the Li counterpart, $Li_2MnP_2O_7$. Using first-principles calculations, we find that the significantly enhanced kinetics of $Na_2MnP_2O_7$ is mainly due to the locally flexible accommodation of Jahn−Teller distortions aided by the corner-sharing crystal structure in triclinic $Na_2MnP_2O_7$. By contrast, in monoclinic $Li_2MnP_2O_7$, the edge-sharing geometry causes multiple bonds to be broken and formed during charging reaction with a large degree of atomic rearrangements. We expect that the similar computational strategy to analyze the atomic rearrangements can be used to predict the kinetics behavior when exploring new cathode candidates.
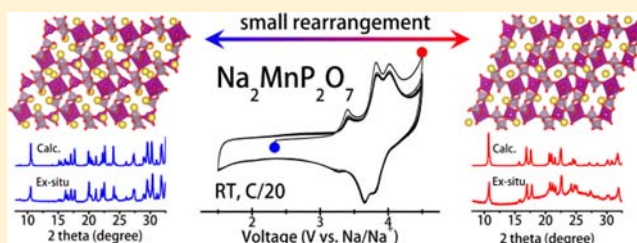
INTRODUCTION

As lithium ion batteries (LIBs) expand their territories from the current mobile electronics to large-scale applications represented by sustainable transportation and stationary energy storage systems (ESSs), the battery community has continuously pursued cheap and abundant active materials that facilitate good performances in energy density, power capability, cycle life, and safety. Particularly for ESS applications in which the amount of readily available resources for active materials is critical, sodium ion batteries (SIBs) have been regarded as a promising alternative to LIBs due to abundance and low price of sodium raw materials.[1−3] However, from the safety perspective, polyanion-based materials that bear strong X−O covalent bonds (X = P, S, B, Si) have received great attention because those bonds are less vulnerable to oxygen evolution and subsequently fire hazard.[4]

On the basis of this background, the research on SIB cathodes has progressed focusing on various polyanion-based cathode materials. Quite naturally, precedent LIB research on the same polyanion-based analogues has given a useful guidance. Recently, among a variety of polyanion-based cathodes, pyrophosphates ($A_2MP_2O_7$, A: alkali ion, M: transition metal) showed promising electrochemical and

thermal properties. On the LIB side, Fe,[5−7] Mn,[7,8] Co,[5] and their multicomponents[7,9,10] have been investigated. The Yamada group first reported decent electrochemical performance of $Li_2FeP_2O_7$ where the material showed 3.5 V vs Li/Li+ with a gravimetric capacity of ~120 mAh g−1.[6] In an effort to raise the operation potential, the Whittingham group tested $Li_2MnP_2O_7$, but found that this material is electrochemically almost ineffective at room temperature due to the sluggish kinetics of the Mn3+/Mn2+ redox couple.[7] A recent study by the Yamada group confirms such sluggish kinetics as the origin of the inactive nature of $Li_2MnP_2O_7$ at room temperature since they observed an activation of otherwise inactive $Li_2MnP_2O_7$ at higher temperatures under slow scan rates.[8] On the SIB side, inspired from the results of the LIB pyrophosphates, several research groups reported $Na_2FeP_2O_7$ as a ~3.0 V SIB cathode alongside its distinctive triclinic crystal structure as opposed to the monoclinic structure of most LIB pyrophosphates.[11−13]

Besides the pyrophosphate, other polyanion-based Mn compounds also usually suffer from far inferior electrochemical performance originating from low electronic conductivity and

poor mobility of phase boundary, which are directly related to the well-known Jahn−Teller distortion of Mn^{3+} as well as large lattice mismatch between the charged and discharged states.[8,9,14] These kinetic barriers have been addressed by the particle size reduction below ~100 nm ($LiMnPO_4$,[15,16] Li_2MnPO_4F,[17] Na_2MnPO_4F,[17] Li_2MnSiO_4[18]) or the increase of operating temperature ($Li_2MnP_2O_7$,[8] Na_2MnPO_4F[19]).

Herein, we report a newly synthesized Mn-based two-sodium pyrophosphate, $Na_2MnP_2O_7$, and its anomalous Mn activation even at room temperature and with relatively large particle sizes, which is completely opposite to the trend in the LIB counterpart. $Na_2MnP_2O_7$ exhibits a clear electrochemical activity in the voltage range of 1.5−4.5 V vs Na/Na^+ with a reversible capacity of ~90 mAh g^{-1} at room temperature, implying substantially enhanced kinetics of the Mn^{3+}/Mn^{2+} redox couple. The observed rate capability of $Na_2MnP_2O_7$ is even comparable to that of the Fe counterpart with excellent cycle performance. This unexpected Mn activation is attributed to its distinctive crystal framework and is further explained by density functional theory (DFT) calculations.

■ RESULTS AND DISCUSSION

Crystal Structure. Two-sodium metal pyrophosphates ($Na_2MP_2O_7$) can crystallize in different polymorphic forms depending on the transition metal (TM) species and synthesis condition. For instance, $Na_2CoP_2O_7$ has been reported to adopt triclinic (*rose*), orthorhombic (*blue*), and tetragonal (ordered-*blue*) structures.[20,21] For the case of M = Cu, two different monoclinic structures, $Na_2CuP_2O_7$-α and -β, were reported.[22] Recently, the Fe-based compound, $Na_2FeP_2O_7$, which is isostructural with the rose-type Co counterpart, was also synthesized and showed excellent electrochemical activity and thermal stability as a SIB cathode.[12] However, unlike most of other TM cases that hold polymorphic phases, for the case of M = Mn, only one type of crystal structure, namely *Mn-ref*, has been found.[23] This fact that there are no other phases reported for $Na_2MnP_2O_7$ is quite surprising since many polyanionic structures that can bear M = Mn, Fe, and Co behave in a similar fashion perhaps due to the similar ionic radii and oxidation states. On the basis of this unusual situation with $Na_2MnP_2O_7$, we suspected the existence of other polymorphic phases of this material and initiated the current investigation. Such expectation indeed led us to find a new $Na_2MnP_2O_7$ phase via a simple conventional solid state reaction process. See the Supporting Information, SI for detailed synthetic procedures.

The X-ray diffraction (XRD) data (Figure 1a) indicate that the as-synthesized $Na_2MnP_2O_7$ adopts a triclinic structure under the space group *P-1*, thus implying that $Na_2MnP_2O_7$ in the present study holds a new crystal structure and is also isostructural with $Na_2FeP_2O_7$ and $Na_2CoP_2O_7$-*rose*. The lattice parameters obtained from a whole pattern fitting are tabulated in Table 1. The lattice constants of $Na_2MnP_2O_7$ turn out to be larger in all of the three directions by 0.06−0.12 Å compared to those of the Fe counterpart perhaps because the ionic radius of Mn^{2+} (0.83 Å) is larger than that of Fe^{2+} (0.78 Å).[24] The inductively coupled plasma (ICP) compositional analyses indicate the atomic ratio of Na:Mn:P = 2.06:1.0:2.13, which is fairly close to the designated stoichiometry of the synthesized compound (Table S1 of the SI).

From the Mn location viewpoint, Mn occupies two different crystallographic sites, octahedral sites (MnO_6) and pyramidal sites (MnO_5) (Figure 1b). Since the two metal sites are in different chemical environments, their redox potentials are
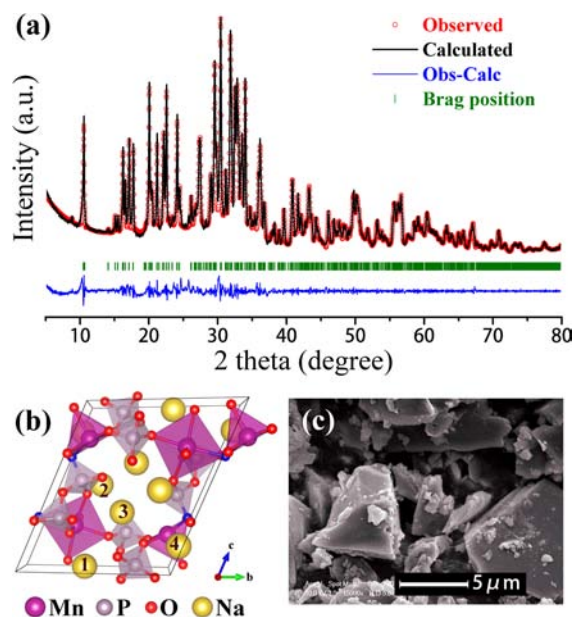

Figure 1. (a) The XRD spectrum and whole pattern fitting of $Na_2MnP_2O_7$ (R_P = 3.18, R_{WP} = 4.59, χ^2 = 2.35). (b) The crystal structure of the triclinic $Na_2MnP_2O_7$ where the purple, gray, red, and yellow spheres represent Mn, P, O, and Na atoms, respectively. The four sodium sites, *Na1−Na4* are also denoted. In this periodic image, the octahedral MnO_6 and pyramidal MnO_5 moieties share one oxygen atom (blue) to make Mn_2O_{10} unit. (c) An SEM image of the as-synthesized sample shows particle sizes in the range of 2−7 μm.

Table 1. Lattice Parameters of $Na_2MnP_2O_7$ and $Na_2FeP_2O_7$

	$Na_2MnP_2O_7$	$Na_2FeP_2O_7$
structure	triclinic *P-1*	triclinic *P-1*
a [Å]	6.5373	6.4338
b [Å]	9.5404	9.4158
c [Å]	11.0735	11.0180
α [°]	64.5664	64.4086
β [°]	79.9632	85.4794
γ [°]	73.4167	72.8073
reference	this work	8

expected to be different as in the cases of the LIB pyrophosphates.[10] As illustrated in Figure 1b, the MnO_6 and neighboring MnO_5 form a Mn_2O_{10} unit by corner-sharing of one oxygen atom (blue sphere in Figure 1b), and each of such unit is separated by PO_4 or P_2O_7. This bonding structure is different from the monoclinic $Li_2MnP_2O_7$ and *Mn-ref* structures in which each metal−oxygen polyhedron edge-shares directly with the neighboring one. As will be shown later, this structural difference (corner sharing vs edge sharing) affects the kinetics dramatically in the actual electrochemical battery tests.

Figures 1c and S1 of the SI are SEM images of the as-synthesized and carbon-coated samples, respectively. The particle sizes of the as-synthesized sample are in the range of 2−7 μm, which are comparable to those of $Li_2MnP_2O_7$.[8] Even after the carbon-coating through a ball-milling process, the particle sizes are still around 1 μm, which is relatively larger than those of the previously reported Mn-based polyanion compounds (<100 nm).[15,17,18]

Electrochemical Measurements. The electrochemical activity of $Na_2MnP_2O_7$ was evaluated by galvanostatic measurements at room temperature (Figure 2a). In the first and

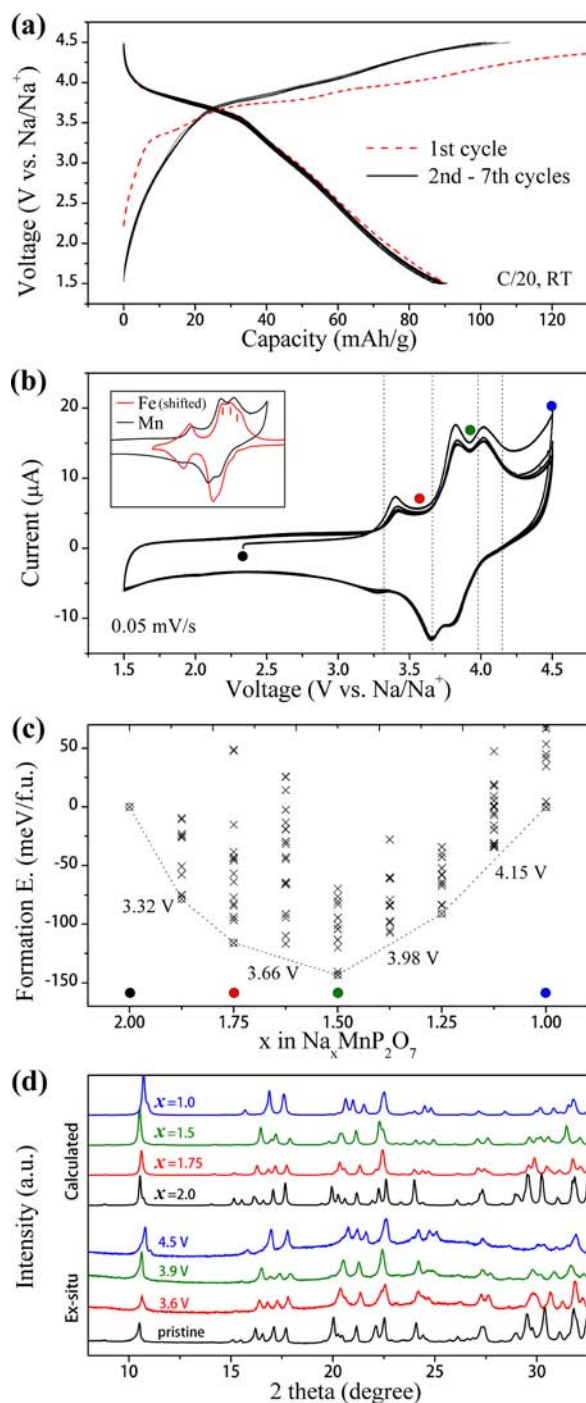**Figure 2.** (a) The galvanostatic charge−discharge curves and (b) CV profiles of $Na_2MnP_2O_7$ measured at room temperature. The CV profiles of $Na_2FeP_2O_7$[12] in the inset of (b) are shifted by 0.85 V for clear comparison. The four dotted lines correspond to the calculated voltages as shown in (c). (c) Calculated formation energies at various compositions and a convex hull for potential calculations. (d) The ex-situ XRD patterns obtained at the potentials marked in (b) together with the simulated patterns at the corresponding compositions marked in (c).

the trend is opposite to typical situations where, for the same polyanion cases, SIB cathodes are often considered to have poorer activities compared to the LIB counterparts. For reference, $Li_2MnP_2O_7$ proved to be completely inactive at room temperature[7] or partially active at 40 °C under a very slow rate of C/50.[8] The ICP data in Table S2 of the SI (atomic ratio of Na:Mn:P = 1.08:1.0:2.17) consistently support the extraction of almost one Na ion at the fully charged state (4.5 V). Although the first charge profile shows a larger capacity compared to those in the subsequent cycles perhaps due to some side reactions associated with surface layer formation, the phase transitions of $Na_2MnP_2O_7$ can be exclusively isolated because the redox peak positions remain identical over repeated cycles as shown in Figure 2b.

In the cyclic voltammetry (CV) measurements (Figure 2b), three oxidation/reduction peaks (3.39/3.26, 3.82/3.65, and 4.02/3.77 V) were observed. Although the number of observed peaks is different from that of the Fe counterpart which showed four oxidation/reduction peaks (inset of Figure 2b),[12] the overall peak shape and peak-to-peak intervals are similar, indicating the similar electrochemical behavior between the two sodium pyrophosphate analogues. The average voltage difference (0.85 V) between $Na_2MnP_2O_7$ and $Na_2FeP_2O_7$ is comparable to that (0.95 V) between $Li_2MnP_2O_7$ and $Li_2FeP_2O_7$, but is larger than the difference (0.65 V) between $LiMnPO_4$ and $LiFePO_4$. Although it appears that the discharge capacity in the potential range below 3.5 V is smaller in the CV data than that in the galvanostatic data, this is mainly due to peak broadening around 3.2 V in the CV data. If a proper baseline is drawn in the CV data, then the capacity turns out to be consistent in both measurements over the entire potential range. For deeper understanding of this material and its phase transformations during electrochemical processes, we performed theoretical calculations and ex-situ XRD measurements.

A series of intermediate phases and their equilibrium potentials were identified by employing DFT calculations (see SI for calculation details).[25−34] In our calculation regime, one single-phase reaction at 3.32 V and three consecutive two-phase reactions at 3.66, 3.98, and 4.15 V were found (Figure 2c). In general, the presence of intermediate phases more stable than the phases at the end of each subregime (formation energies at the intermediate phases are located below the dotted line) indicates favorable character of single-phase reactions. Likewise, the other cases that include no stable intermediate phases prefer two-phase reactions. Most of the calculated potentials are consistent with the average oxidation/reduction peak locations observed in the CV measurement and are presented as dotted lines in Figure 2b. The almost invisible peak at 4.15 V could be attributed to the situation that the redox peak is buried by the polarization, and requires further investigation for clear understanding. The overall phase behavior of $Na_2MnP_2O_7$ is very similar to that of $Na_2FeP_2O_7$,[12] implying that while the TM species have a strong effect on the redox potential and kinetics, the phase transformation during Na (de)intercalation is persistent regardless of the TM species.

Figure 2d shows the XRD patterns of the pristine, 3.6, 3.9, and 4.5 V samples as well as the Boltzmann averaged XRD patterns at each Na composition (x value) obtained from the calculated structures in Figure 2c. The simulated patterns at x = 2.0, 1.75, 1.5, and 1.0 match well with the experimental patterns measured at the corresponding potentials. These results also support the extraction of one Na ion at the fully charged state, in addition to the structural consistency between experiments

subsequent cycles, a reversible capacity of ∼90 mAh g^{-1} was obtained in the voltage range of 1.5−4.5 V (vs Na/Na$^+$) at a rate of C/20, indicating that 0.9 Na ion per each formula unit of $Na_2MnP_2O_7$ is electrochemically active based on the theoretical capacity of 97.5 mAh g^{-1}. This activity is quite remarkable since

and calculations. On the basis of the well-reproduced calculation results, we developed a more detailed view on the Na extraction sequence and the most probable Na ordering at each composition (Figure S2 of the SI). Following the same notation in Figure 1b, it is anticipated that Na ions are first extracted from half of the *Na1* sites and then sequentially from all of the *Na3* sites and last from half of the *Na4* sites. Therefore, the Na occupancies in the *Na1*, *Na2*, *Na3*, and *Na4* sites are 0.5, 1, 0, and 0.5, respectively, at the fully charged state.

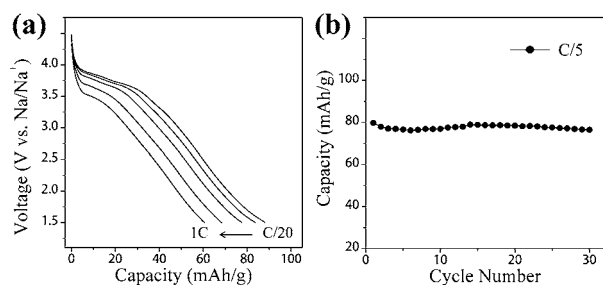$Na_2MnP_2O_7$ exhibits good rate capability (Figure 3a) and cycling performance (Figure 3b). Even when the c-rate

Figure 3. (a) The rate capability of $Na_2MnP_2O_7$ at various C-rates during discharge and (b) discharge cycle life of $Na_2MnP_2O_7$ measured at C/5. In (a), the discharge rates are C/20, C/10, C/5, C/2, 1C from right to left.

increases by 20 times from C/20 to 1C, the original capacity of 88 mAh g^{-1} drops only to 61 mAh g^{-1}. This value corresponds to 69% capacity retention, which is indeed comparable to the 74% retention of the Fe-based counterpart in the same c-rate increase. In addition, the capacity is well preserved over cycling such that 96% of the initial capacity (80 mAh g^{-1}) is retained after 30 cycles when measured at C/5, indicating that sodium (de)intercalation in this material is quite reversible. Considering the relatively large particle sizes around ~1 μm, these electrochemical results at room temperature clearly suggest extraordinary activity of the Mn^{2+}/Mn^{3+} redox couple in this material, especially compared against the Li counterpart that exhibits negligible activity at room temperature. In the next section, such distinctive behavior is discussed in detail focusing on the kinetics and structural properties of both pyrophosphates.

Structural Rearrangements and Mn Kinetics. Several factors have been raised in literature as main reasons for the poor electrochemical activity or large polarization of the Mn-based cathodes: slow phase boundary mobility,[35] large lattice mismatch,[14] low electronic conductivity,[8,9,14,35] large volume strain,[8] strong Jahn–Teller distortion,[8,9,35] large effective mass of polaron,[16,36] and lack of minority nonbonding electrons.[9] In fact, we interpret that all of these factors are correlated with each other as summarized in Scheme 1. In essence, all previously proposed mechanisms for the Mn-inactivity are related to structural reorganization in one way or the other as follows:

(1) Since the electron for the Mn^{3+}/Mn^{2+} redox couple originates from the antibonding orbital ($e_g^\uparrow$), during the relevant redox reactions the corresponding M−O bond lengths change more than those in the Fe^{3+}/Fe^{2+} couple cases where a transferring electron comes from the nonbonding orbital ($t_{2g}^\downarrow$).[37] (2) The Mn^{3+} in the high spin state ($t_{2g}^3 e_g^1$) is preferred to undergo Jahn–Teller distortion that is well-known to stabilize the structures by breaking symmetry of orbitals.

Scheme 1. Effects of Electronic Structures on the Kinetics of Mn-Based Cathode Materials
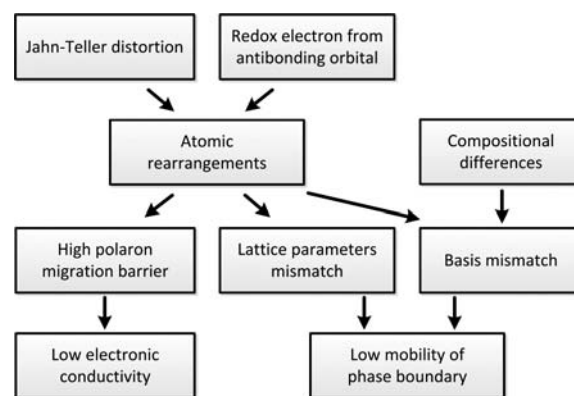
These unique electronic structures lead to significant rearrangements in the positions of metal and oxygen atoms as well as resultant changes in their bond lengths during electrochemical reactions. (3) The band gap of $Na_2MnP_2O_7$ turns out to be larger than 5 eV (Figure S3 of the SI), implying that the electron conduction mechanism in $Na_2MnP_2O_7$ is probably a polaron migration as in the olivine-type phosphates.[38,39] For the latter band gap calculation, we note that we used a hybrid functional[40] which was proven to give quite accurate electronic structures for Mn-based materials.[14,37] In this concept, the polaron migration barrier is strongly affected by the propagation of local structural deformations since the electron transfer occurs adiabatically after the distortion of M−O geometry,[39,41] indicating that the large structural distortions with potentially large reorganization energy can deteriorate the electron transfer kinetics.[16,36] (4) A slow mobility of phase boundary is associated with the structural and compositional mismatches between charged and discharged phases. Although the structural mismatch is typically referred to the lattice parameters mismatch, the basis mismatch, such as mismatch in the atomic positions, should also be considered since the atomic positions and their bond structures can still be altered drastically without noticeable lattice parameters evolution which can impose significant kinetic barriers.

Therefore, on the basis of these considerations, it can be deduced that the degree of detailed atomic rearrangement during charging and discharging can be a key metric to predict and explain the kinetics of various Mn-based cathode materials. To this end, again, the variations of atomic positions and their bond lengths should be considered beyond the simple evaluation of the volume and lattice parameters. Hence, we calculated the displacements of Mn, P, and O atoms and the changes of M−O, P−O bond lengths of $A_xMP_2O_7$ (A = Li and Na, M = Fe and Mn) for the charged ($x = 1$) and discharged ($x = 2$) states. These parameter changes were used to evaluate the effects of TMs (Fe vs Mn) and structures (monoclinic $Li_2MP_2O_7$ vs triclinic $Na_2MP_2O_7$) on the battery activity.

Figure 4a,b show the displacements of Mn and O atoms, respectively, at their various positions between the fully charged and discharged states, and the average values are listed in Table 2. Hereafter, the displacement of each element is defined as a distance between the initial and final locations (between the charged and discharged states in the current case). For the TM position (ΔM in Table 2), in $Li_2MP_2O_7$ the displacements of the Mn atoms are much larger than those of the Fe atoms by a factor of 3−4. But, for $Na_2MP_2O_7$, the displacements of both
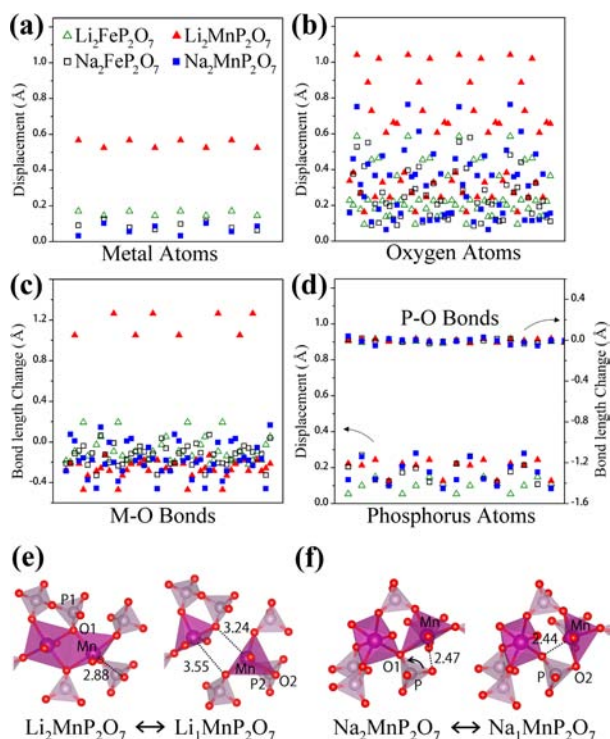
Figure 4. Displacements of (a) TMs and (b) oxygen-atoms, and (c) M-O bond length changes for $A_2MP_2O_7$ (A = Li and Na, M = Fe and Mn) during full charging. The x-axes in (a-c) correspond to the different crystallographic sites of the relevant elements. (d) The displacements of phosphorus atoms (left) and P−O bond length changes (right). For the different samples, the same color codes are used for (b−d) as in (a). The rearrangements of atomic positions and their bond lengths between the charged and discharged states for (e) $Li_2MnP_2O_7$ and (f) $Na_2MnP_2O_7$. Atomic colors are the same as in Figure 1a and the numbers are M−O distances in Å.

Table 2. Average Values for the Displacements of Metal (ΔM), Oxygen (ΔO), and Phosphorus (ΔP) for Each Compound between the Charged and Discharged States[a]

Δ(Å)	$Li_2FeP_2O_7$	$Li_2MnP_2O_7$	$Na_2FeP_2O_7$	$Na_2MnP_2O_7$
ΔM	0.159	0.546	0.090	0.070
ΔO	0.265	0.542	0.251	0.316
|ΔM−O|	0.139	0.412	0.138	0.194
ΔP	0.103	0.201	0.165	0.172
|ΔP−O|	0.015	0.011	0.014	0.018

[a]The absolute averages of bond length changes (ΔM−O and ΔP−O) are also presented.

TM elements are quite small and nearly the same. For the oxygen atoms bonded to TMs, due to the aforementioned Jahn−Teller distortion and antibonding character of the redox electrons, the Mn-based materials show significantly larger displacements compared to those of the Fe counterparts in both lithium and sodium pyrophosphates. More interestingly, for the same TMs, $Na_2MP_2O_7$ shows smaller displacements for oxygen atoms than those of $Li_2MP_2O_7$, suggesting easier accommodation of Jahn−Teller distortions in $Na_2MP_2O_7$ compared to $Li_2MP_2O_7$.

The superior electrochemical activity of $Na_2MnP_2O_7$ is most clearly reflected in the M−O bond length changes (Figure 4c and Table 2) and associated bond breaking and forming. The average change of the M−O bond lengths in $Li_2MnP_2O_7$ is

0.412 Å where several M−O bonds in the calculation unit cell elongate by even more than 1 Å, implying the M−O bond cleavages. In fact, when charging occurs (Figure 4e), the two edge-sharing Mn−O bonds are completely ruptured and one new bond is formed to accommodate Jahn−Teller distortion and also to minimize the electrostatic repulsion between Mn^{3+} ions. As a result, a pair of octahedral and pyramidal TM polyhedrons is disjointed into two pyramidal-like polyhedrons.

By contrast, the average change of the M−O bond lengths in $Na_2MnP_2O_7$ is only 0.194 Å, which is comparable to the changes in $Li_2FeP_2O_7$ and $Na_2FeP_2O_7$. In the case of $Na_2MnP_2O_7$ (Figure 4f), the atomic rearrangements are much more localized and bonds before and after the deintercalation reaction are even difficult to characterize as broken or newly created. When bonds are broken and created, typically some fraction of bond energy that is broken is required as an activation energy. For example, for an atom transfer reaction of the type AB + C → A + BC, very roughly 10% of the AB bond energy is needed as an activation barrier. Therefore, unlike $Na_2MnP_2O_7$ without any noticeable changes in bonding, for $Li_2MnP_2O_7$, rupturing of two bonds and creation of one bond for a given Mn_2O_{10} unit would produce substantial kinetic barrier which makes the deintercalation reaction unlikely to occur at room temperatures (but can be made possible at higher temperatures as shown in reference 8).

To be more specific about the structural evolutions, the electrostatic repulsion between Mn^{3+} ions can be responsible for the bond cleavages in $Li_2MnP_2O_7$, but it is not a dominant factor since (1) the drastic bond cleavage is not observed in $Li_2FeP_2O_7$ which undergoes the same electrostatic repulsion and (2) the distance between Mn ions are rather reduced for charging from $Na_2MnP_2O_7$ (3.86 Å) to $Na_1MnP_2O_7$ (3.68 Å). Instead, the Jahn−Teller distortion is a more direct reason to lead to the structural evolutions. One would expect that the Mn sites in $Na_2MnP_2O_7$ would undergo the same Jahn−Teller distortion as in the $Li_2MnP_2O_7$, but it appears that the corner-sharing in $Na_2MnP_2O_7$, rather than edge-sharing, gives more degree of freedom to accommodate distortions and makes the effects of Jahn−Teller distortion more localized on each Mn site only. In addition, while the PO_4 bonds are quite strong and do not change to any significant degree for both $Li_2MnP_2O_7$ and $Na_2MnP_2O_7$ (Figure 4d), they can act as hinges to accommodate distortions for $Na_2MnP_2O_7$. For example (arrow in Figure 4f), the Mn−O1−P and Mn−O2−P bonds are slightly lengthened and shortened during charging due to a simple rotation of the bridging PO_4 polyhedron. We note that there are other Mn-based cathode materials such as $LiMnPO_4$,[15,16] Li_2MnSiO_4,[18] and Na_2MnPO_4F,[19] and thus, as a future study, it would be helpful to assess whether the proposed atomic rearrangement metric can also be a proper descriptor for the kinetics evaluation for the related materials.

We also note that the ionic channel structure can play a role in the improved kinetics of $Na_2MnP_2O_7$. The three-dimensional Na ion channels in $Na_2MnP_2O_7$ can offer more efficient paths for ionic diffusion compared to the two-dimensional channels in $Li_2MnP_2O_7$.

■ CONCLUSIONS

We synthesized a new $Na_2MnP_2O_7$ polymorph as an SIB cathode material and report its structural and electrochemical properties. It adopts a triclinic crystal framework under the space group of *P-1*. This Mn-based material exhibits unexpected electrochemical activity at room temperature, including good

performance in the capacity, rate capability, and cycle life. The observed activity of $Na_2MnP_2O_7$ is far superior to that of the almost inactive Li counterpart (monoclinic $Li_2MnP_2O_7$) and is even comparable to that of $Na_2FeP_2O_7$. On the basis of first-principles calculations and detailed atomic structures, we were able to correlate the improved kinetics of $Na_2MnP_2O_7$ with the small extent of atomic rearrangements, which lower the barriers for electron conduction and phase boundary migration. This can be compared against $Li_2MnP_2O_7$ that has multiple bonds that are broken during charging and hence substantial activation barrier. Therefore, we propose the degree of the atomic rearrangement as a key metric for the evaluation of kinetics of various cathode materials. It is also noteworthy that there exist 6 different crystal structures for $Na_2MP_2O_7$ compounds (*M = 3d* TMs), and we have identified only one of them, $Na_2CoP_2O_7$-*rose* type structure, in the present study. Thus, it is expected that the other polymorphic structures are also available for unreported TM species and, hopefully, they may also show unexpected characteristics such as the anomalous Mn activation shown here.

■ ASSOCIATED CONTENT

ⓢ Supporting Information
Experimental procedures, details of DFT calculations, ICP−MS data, SEM, Sodium ordering for each composition, Density of states. This material is available free of charge via the Internet at http://pubs.acs.org.

■ AUTHOR INFORMATION

Corresponding Author
ysjn@kaist.ac.kr, jangwookchoi@kaist.ac.kr
Author Contributions
||These authors contributed equally to this work.
Notes
The authors declare no competing financial interest.

■ ACKNOWLEDGMENTS

■ REFERENCES

(1) Kim, S.-W.; Seo, D.-H.; Ma, X.; Ceder, G.; Kang, K. *Adv. Energy Mater.* **2012**, *2*, 710.
(2) Palomares, V.; Serras, P.; Villaluenga, I.; Hueso, K. B.; Carretero-Gonzalez, J.; Rojo, T. *Energy Environ. Sci.* **2012**, *5*, 5884.
(3) Slater, M. D.; Kim, D.; Lee, E.; Johnson, C. S. *Adv. Funct. Mater.* **2012**, DOI: 10.1002/adfm.201200691.
(4) Gong, Z.; Yang, Y. *Energy Environ. Sci.* **2011**, *4*, 3223.
(5) Kim, H.; Lee, S.; Park, Y.-u.; Kim, H.; Kim, J.; Jeon, S.; Kang, K. *Chem. Mater.* **2011**, *23*, 3930.
(6) Nishimura, S.-i.; Nakamura, M.; Natsui, R.; Yamada, A. *J. Am. Chem. Soc.* **2010**, *132*, 13596.
(7) Zhou, H.; Upreti, S.; Chernova, N. a.; Hautier, G.; Ceder, G.; Whittingham, M. S. *Chem. Mater.* **2011**, *23*, 293.
(8) Tamaru, M.; Barpanda, P.; Yamada, Y.; Nishimura, S.-i.; Yamada, A. *J. Mater. Chem.* **2012**, *22*, 24526.
(9) Furuta, N.; Nishimura, S.-i.; Barpanda, P.; Yamada, A. *Chem. Mater.* **2012**, *24*, 1055.
(10) Shakoor, R. A.; Kim, H.; Cho, W.; Lim, S. Y.; Song, H.; Lee, J. W.; Kang, J. K.; Kim, Y.-T.; Jung, Y.; Choi, J. W. *J. Am. Chem. Soc.* **2012**, *134*, 11740.
(11) Honma, T.; Togashi, T.; Ito, N.; Komatsu, T. *J. Ceram. Soc. Jpn.* **2012**, *120*, 344.
(12) Kim, H.; Shakoor, R. a.; Park, C.; Lim, S. Y.; Kim, J.-S.; Jo, Y. N.; Cho, W.; Miyasaka, K.; Kahraman, R.; Jung, Y.; Choi, J. W. *Adv. Funct. Mater.* **2012**, DOI: 10.1002/adfm.201201589.
(13) Barpanda, P.; Ye, T.; Nishimura, S.-i.; Chung, S.-C.; Yamada, Y.; Okubo, M.; Zhou, H.; Yamada, A. *Electrochem. Commun.* **2012**, *24*, 116.
(14) Ong, S. P.; Chevrier, V. L.; Ceder, G. *Phys. Rev. B* **2011**, *83*, 075112.
(15) Qin, Z.; Zhou, X.; Xia, Y.; Tang, C.; Liu, Z. *J. Mater. Chem.* **2012**, *22*, 21144.
(16) Yonemura, M.; Yamada, A.; Takei, Y.; Sonoyama, N.; Kanno, R. *J. Electrochem. Soc.* **2004**, *151*, A1352.
(17) Kim, S.-W.; Seo, D.-H.; Kim, H.; Park, K.-Y.; Kang, K. *Phys. Chem. Chem. Phys.* **2012**, *14*, 3299.
(18) Dominko, R. *J. Power Sources* **2008**, *184*, 462.
(19) Wu, X.; Zheng, J.; Gong, Z.; Yang, Y. *J. Mater. Chem.* **2011**, *21*, 18630.
(20) Sanz, F.; Parada, C.; Rojo, J. M.; Ruiz-Valero, C.; Saez-Puche, R. *J. Solid State Chem.* **1999**, *145*, 604.
(21) Erragh, F.; Boukhari, A.; Elouadi, B.; Holt, E. M. *J. Crystallogr. Spectrosc. Res.* **1991**, *21*, 321.
(22) Erragh, F.; Boukhari, A.; Abraham, F.; Elouadi, B. *J. Solid State Chem.* **1995**, *120*, 23.
(23) Huang, Q.; Hwu, S.-J. *Inorg. Chem.* **1998**, *37*, 5869.
(24) Shannon, R. D. *Acta Crystallogr., Sect. A* **1976**, *32*, 751.
(25) Perdew, J. P.; Burke, K.; Ernzerhof, M. *Phys. Rev. Lett.* **1996**, *77*, 3865.
(26) Blochl, P. E. *Phys. Rev. B* **1994**, *50*, 17953.
(27) Kresse, G.; Fruthmuller, J. *Comput. Mater. Sci.* **1996**, *6*, 15.
(28) Dudarev, S. L.; Botton, G. A.; Savrasov, S. Y.; Humphreys, C. J.; Sutton, A. P. *Phys. Rev. B* **1998**, *57*, 1505.
(29) Zhou, F.; Cococcioni, M.; Marianetti, C.; Morgan, D.; Ceder, G. *Phys. Rev. B* **2004**, *70*, 1.
(30) Monkhorst, H. J.; Pack, J. D. *Phys. Rev. B* **1976**, *13*, 5188.
(31) Momma, K.; Izumi, F. *J. Appl. Crystallogr.* **2008**, *41*, 653.
(32) Van der Ven, A.; Aydinol, M. K.; Ceder, G.; Kresse, G.; Hafner, J. *Phys. Rev. B* **1998**, *58*, 2975.
(33) Toukmaji, A. *Comput. Phys. Commun.* **1996**, *95*, 73.
(34) Aydinol, M. K.; Kohan, A. F.; Ceder, G.; Cho, K.; Joannopoulos, J. *Phys. Rev. B* **1997**, *56*, 1354.
(35) Gwon, H.; Seo, D.-H.; Kim, S.-W.; Kim, J.; Kang, K. *Adv. Funct. Mater.* **2009**, *19*, 3285.
(36) Yamada, A.; Kudo, Y.; Liu, K.-Y. *J. Electrochem. Soc.* **2001**, *148*, A747.
(37) Johannes, M. D.; Hoang, K.; Allen, J. L.; Gaskell, K. *Phys. Rev. B* **2012**, *85*, 115106.
(38) Zaghib, K.; Mauger, A.; Goodenough, J. B.; Gendron, F.; Julien, C. M. *Chem. Mater.* **2007**, 3740.
(39) Ellis, B.; Perry, L. K.; Ryan, D. H.; Nazar, L. F. *J. Am. Chem. Soc.* **2006**, *128*, 11416.
(40) Heyd, J.; Scuseria, G. E.; Ernzerhof, M. *J. Chem. Phys.* **2006**, *124*, 219906.
(41) Maxisch, T.; Zhou, F.; Ceder, G. *Phys. Rev. B* **2006**, *73*, 104301.